Environmental Science & Technology

pubs.acs.org/est

Article

Phase State and Relative Humidity Regulate the Heterogeneous Oxidation Kinetics and Pathways of Organic-Inorganic Mixed Aerosols

Chuanyang Shen, Wen Zhang, Jack Choczynski, James F. Davies, and Haofei Zhang*

Cite This: *Environ. Sci. Technol.* 2022, 56, 15398−15407

Read Online

ACCESS | Metrics & More | Article Recommendations | Supporting Information

ABSTRACT: Inorganic species always coexist with organic materials in atmospheric particles and may influence the heterogeneous oxidation of organic aerosols. However, very limited studies have explored the role of the inorganics in the chemical evolution of organic species in mixed aerosols. This study examines the heterogeneous oxidation of glutaric acid−ammonium sulfate and 1,2,6-hexanetriol−ammonium sulfate aerosols by hydroxyl radicals (OH) under varied organic mass fractions (f_{org}) and relative humidity in a flow tube reactor. Coupling the oxidation kinetics and product measurements with kinetic model simulations, we found that under both low relative humidity (RH, 30−35%) and high RH conditions (85%), the decreased f_{org} from 0.7 to 0.2 accelerates the oxidation of the organic materials by a factor of up to 11. We suggest that the faster oxidation kinetics under low-RH conditions is due to full or partial phase separation, with the organics greatly enriched at the particle outer region, while enhanced "salting-out" of the organics and OH adsorption caused by higher inorganics could explain the observations under high-RH conditions. Analysis of the oxidation products reveals that the dilution of organics by the inorganic salts and corresponding water uptake under high-RH conditions will favor alkoxy radical fragmentation by a factor of 3−4 and inhibit its secondary chain propagation chemistry. Our results suggest that atmospheric organic aerosol oxidation lifetime and composition are strongly impacted by the coexistent inorganic salts.

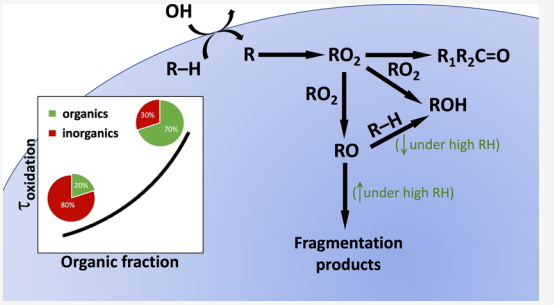

KEYWORDS: *phase separation, salt out, alkoxy radical, fragmentation, aerosol lifetime*

Downloaded via UNIV OF CALIFORNIA RIVERSIDE on May 7, 2024 at 23:21:23 (UTC).
See https://pubs.acs.org/sharingguidelines for options on how to legitimately share published articles.

INTRODUCTION

Atmospheric aerosol particles are mainly composed of organic and inorganic materials, in which the organics may account for 20−70% of total aerosol mass.[1] As the atmosphere is a highly oxidizing environment in the presence of gas-phase oxidants such as hydroxyl radicals (OH), the organic materials at the particle surface undergo heterogeneous oxidation processes,[2] which may transform the aerosol particles' chemical compositions and the physical properties, including aerosol size and volume,[3] optical properties,[4] hygroscopicity,[5,6] and cloud condensation nuclei activity.[7] The two key aspects in aerosol heterogeneous oxidation processes are the oxidation rates and reaction pathways, which together govern the aerosol composition through oxidation. The reaction rates describe how fast the organic materials are degraded and the reaction pathways determine the bulk organic compositions.[3] The various reaction pathways of the peroxy radicals (RO_2) and alkoxy radicals (RO) following the initial OH-oxidation (Figure 1) determine how the parent organic molecules undergo functionalization and fragmentation and hence affect the chemical composition and mass evolution.[8] Extensive studies have examined these two aspects for pure organic particles and provided crucial information on the reactivities and compositions of organic aerosols during heterogeneous OH-oxidation.[3,9−15]

However, pure organic particles rarely exist in the atmosphere, especially in regions influenced by human activity.[16] In the presence of inorganic salts, the particle's water content and phase state may be significantly changed.[17−20] As a result, the heterogeneous oxidation of organic-inorganic mixed particles could be largely different. Despite the strong atmospheric relevance, few studies have investigated the heterogeneous OH-oxidation of organic-inorganic mixtures.[21−23] Among the limited studies, it was found that the heterogeneous oxidation rates are increased when the organics and inorganics are fully phase-separated and the organic surface-to-volume ratio is enhanced[21] but are reduced when the organics and inorganics form a well-mixed single liquid phase due to surface dilution.[22] These conflicting

Received: June 28, 2022
Revised: October 18, 2022
Accepted: October 19, 2022
Published: October 28, 2022

ACS Publications

© 2022 American Chemical Society

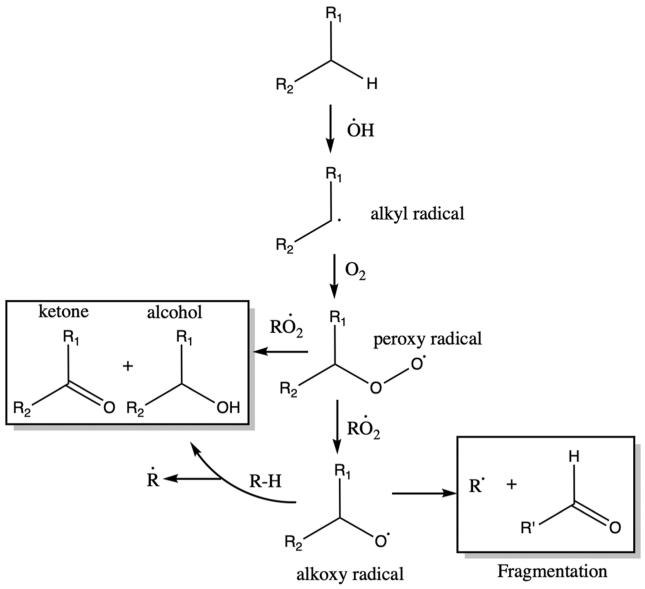

Figure 1. Reaction mechanism for the heterogeneous OH oxidation of organic species in the particle phase.

results suggest that relative humidity (RH) and particle phase states may play a pivotal role in heterogeneous oxidation of organic-inorganic mixed aerosols. For less polar organics, they often present a clear phase-separated structure when mixed with inorganic salts, which has been the focus in most previous organic−inorganic mixture heterogeneous oxidation studies.[21,24,25] But most organic aerosols are more polar in the real atmosphere[1] and have lower or no separation RH when mixed with inorganic salts.[17,26,27] However, when organic-inorganic mixed particles are dried, especially when undergoing nonequilibrium efflorescence, spatial heterogeneity may occur due to sequential efflorescence caused by the differences in individual nucleation rates and transporting processes. Under this condition, they can be present in amorphous phase state, rather than the well-defined, phase-separated, or well-mixed phase state.

Despite the modified oxidation kinetics, previous studies suggested that the OH-initiated heterogeneous oxidation mechanism and products of organic-inorganic mixed particles are qualitatively similar to those of pure organic particles.[22,28] However, the effects of inorganic salts, phase states, and particle water on the heterogeneous oxidation pathways and products remain elusive. In this study, we investigate OH-initiated heterogeneous oxidation of organic-inorganic mixed aerosols using glutaric acid (GTA) and 1,2,6-hexanetriol (HXT) as the model organic materials and ammonium sulfate (AS) as the model inorganic salt. GTA has an O/C ratio of 0.8 and is studied to represent the highly oxidized organic aerosols in the atmosphere, whereas HXT has an O/C ratio of 0.5, representative of the moderately oxidized organic aerosols. The functional groups in these two model compounds (i.e., carboxylic acid and alcohol) are also often found in ambient organic aerosols.[29] Heterogeneous OH oxidation experiments are performed for the mixed particles with varied organic mass fractions (f_{org}) in the relevant 0.2−0.7 range and under both low RH (30−35%) and high RH (85%).

MATERIALS AND METHODS

Chemicals and Reagents. The chemicals and reagents used in this study and their purities and suppliers are as follows: glutaric acid (Sigma-Aldrich, 99%), 1,2,6-hexanetriol (TCI, >96%), ammonium sulfate (Fisher Chemical, 99.8%), ammonium chloride (Fisher Chemical, >99.0%), toluene (Certified ACS, 99.9%), pyridine (DriSolv., 99.8%), BSTFA W/1% TMCS (Restek Corporation), sodium chloride (Sigma-Aldrich, 99.5%), and acetonitrile (HPLC Grade Fisher Chemical, >99.9%). All chemicals were used without further purification.

Experimental Details. All the heterogeneous OH oxidation experiments of organic-inorganic aerosol mixtures were performed in a laminar flow tube reactor (FTR, Quartz, 1.02 m long, 7.19 cm i.d., and volume ~4.12 L) at room temperature (20−25 °C).[15] The experimental setup is illustrated in the Supporting Information (SI), Figure S1. A total inlet flow of 4 L min^{-1} was used in all experiments. A zero-air generator (Aadco Instrument, Inc., 747-30) was used to supply clean dry and wet air flows to achieve the RH of 30−35% or 85%, measured by an RH sensor (Omega Inc., RH-USB). The wet flow was generated by passing the dry air through a heated jar containing deionized water. O_3 was introduced into the FTR by an O_3 generator (Ozone Solutions Inc). The OH radicals were formed through photolysis of O_3 with two 254 nm UV lamps in the presence of water vapor.[3,14,15] The OH exposure levels were simulated using a photochemical kinetic box model based on O_3 concentrations before and after UV illumination[30] and were controlled at 0.2−3.0 × 10^{12} molecules cm^{-3}. Organic-AS mixed aerosol particles were generated by a constant output atomizer (TSI Inc.) using solutions with a total concentration of 2 g L^{-1} and varied f_{org} (0.2−0.7). In two experiments, GTA was mixed with both AS and ammonium chloride (ACl) to study the effects of different inorganic species. The peak diameter of output particles varied from 70 to 100 nm. O_3 concentrations in the FTR were measured by an O_3 analyzer (Thermo Environmental Instruments, Model 49C). A scanning electrical mobility scanner and a mixing condensation particle counter (SEMS and MCPC, Brechtel Manufacturing Inc.) were used to measure size distribution and number concentration of the mixed particles from 10 to 900 nm. After the particle mass concentrations and ozone concentrations became stable, particle samples were collected using a spot sampler (Aerosol Devices Inc.) at 1.5 L min^{-1} for 10−20 min.

All the collected samples were immediately dissolved in a 170 μL mixture of toluene, acetonitrile, pyridine, and BSTFA (volume ratio of 1:3:3:10) for gas chromatograph electron impact ionization mass spectrometry (GC-EI-MS) analysis, or in 200 μL acetonitrile with 0.1 mM NaCl for electrospray ionization (ESI) ion mobility spectrometry time-of-flight mass spectrometry (IMS-TOF) analysis. The detailed description of the instruments can be found in our previous work.[14,31−35] For the GC-EI-MS (Agilent Inc., 7890 GC and 5975 MSD) analysis, the extracted samples were subjected to BSTFA derivatization at 70 °C for 1 h, which converts alcohol groups (−OH) to trimethylsilyl (-*O*-Si$(CH_3)_3$) groups. Thus, GTA, HXT, sulfate, and many oxidation products that contain carboxylic acid and −OH groups can be derivatized to become detectable by the GC-EI-MS. IMS-TOF (Tofwerk Inc.) was used to supplement the GC-EI-MS for measuring a more comprehensive spectrum of products that are not detectable in

https://doi.org/10.1021/acs.est.2c04670
Environ. Sci. Technol. 2022, 56, 15398−15407

the GC-EI-MS. IMS resolution is $(t/\Delta t) \sim 100$, and the TOF mass resolution is $(m/\Delta m) \sim 4000$.

Single Particle Levitation Studies. Phase changes in particles containing AS and GTA were explored in levitated particles using a linear-quadrupole electrodynamic balance (LQ-EDB).[36] Sample solutions were prepared at an aqueous concentration of ~5 g L^{-1}, and droplets with a diameter on the order of 50 μm were generated using a microdroplet dispenser (Microfab MJ-ABP-01) and introduced into the LQ-EDB. The droplets were inductively charged with up to 50 fC at the point of generation and became confined within the electric fields.[37] The excess water evaporated, and the resulting particles attained equilibrium with the chamber RH with a diameter on the order of 10 μm. Mie resonance spectra were measured by illumination with a red LED, as described in our previous work,[36] to determine the size and refractive index of the sample. The evolution of the Mie resonance spectra was used to infer changes in the size, optical properties, and morphology of the particles as the RH varied. The change in the relative size of the particle was also measured using the voltage required to balance the particle. Given the introduction of airflow at ~10 cm s^{-1}, the Stokes drag force was much larger than the weight of the particle, and the electrostatic force was proportional to the diameter of the particle. This allows the influence of RH on dried particles to be measured in the absence of clear Mie resonance spectra.

Kinetic Simulations. To explain the observed oxidation kinetics, a reaction-diffusion multilayer kinetic model was developed, as described in our previous work,[15] which is essentially a similar representation to several other model frameworks that have simulated aerosol heterogeneous oxidation chemistry.[38−40] The model constructs a multicompartment rectangular prism to approximate the aerosol particle, while maintaining the same surface-to-volume ratio of the spherical aerosol and hence preserving the relevant scaling between surface and bulk processes. The organic diffusion coefficients (D_{org}) under all the experimental conditions are estimated using the AIOMFAC model to first obtain the viscosity (η) of the parent OA.[41,42] Then, D_{org} can be calculated based on the Stokes−Einstein equation:

$$D_{org} = \frac{k_B \times T}{6\pi \times a \times \eta} \quad (1)$$

where k_B is the Boltzmann constant; T is the temperature, and a is the effective molecular radius (estimated by the molecular weight and density). The η values in the model remain constant for each organic-inorganic condition for simplicity, similar to previous studies.[15,39,40] Using this method, we estimate that the D_{org} values for the GTA-AS mixtures under 35% RH have a range of 1.0×10^{-12}−2.1×10^{-8} cm^2 s^{-1} depending on the phase state (discussed later) and f_{org}. In comparison, the D_{org} values for the GTA-AS mixtures under 85% have a range of 8.6×10^{-7}−2.0×10^{-6} cm^2 s^{-1}, varied by f_{org}. Similarly, the D_{org} value for the HXT-AS mixtures under 30% RH is 7.8×10^{-10} cm^2 s^{-1} and may range from 1.5×10^{-6}−2.6×10^{-6} cm^2 s^{-1} under 85% RH, varied by f_{org}.

Under the low-RH conditions, the particle-phase diffusion may be slow for both mixed aerosol systems. Thus, the multicompartment configuration is necessary. The thickness of each compartment is set to 1 nm, which was suggested to be a good representation of semisolid aerosol particles.[40] Each compartment is assumed to be a well-mixed volume. The model includes (1) the adsorption, desorption, and reactions of OH at the surface compartment of the particles; (2) organic radical-centered and multigenerational reactions in each compartment; and (3) diffusions of all the species molecules between adjacent compartments. The adsorption of OH is given by

$$k_{ads} = \frac{\alpha \times \bar{c} \times A \times f_{site}}{4 \times V_s} \quad (2)$$

where k_{ads} is the pseudo first-order adsorption rate (s^{-1}); α is the surface sticking coefficient; $\bar{c}$ is the mean thermal speed of OH (cm s^{-1}); A is the aerosol surface area (cm^2); f_{site} is the fraction of available surface sites for OH adsorption (= available site number/maximum site number);[38,39] and V_s is the volume of the surface layer (cm^3). The desorption rate constant for OH is fixed at 2.86×10^{10} s^{-1}, consistent with its estimated lifetime on aqueous surfaces.[40] The evaporation of a major fragmentation product, oxalic acid, is also considered in the model.[43] The second-order reaction rates of GTA with OH (k_{GTA+OH}) are based on recent studies of aqueous-phase GTA + OH reactions.[44] The second-order reaction rate constants for OH with HXT (k_{HXT+OH}) and all the oxidation products are estimated using the structure−activity relationship (SAR) for aqueous-phase oxidation.[45,46] The model also explicitly represents the chemical reactions for GTA, which includes functionalization reactions up to the second generation and all fragmentation reactions (Figure S2). The HXT oxidation mechanism is more simplified to only represent the generic oxidation pathways but is sufficient to simulate HXT degradation. The rate constants for RO_2- and RO-involved reactions (shown in Figure 1) are from previously published work.[39,40,47] Details of the reactions in the model can be found in Table S1.

Under 85% RH, the organic-inorganic mixed aerosols are assumed to be a well-mixed aqueous system with instantaneous mixing. Thus, a single bulk compartment is used in the model to reduce computational costs.[39] Moreover, with the aqueous-phase aerosols that contain carboxylic acids, it has been shown that acid−base may occur concurrently with the organic radical chemistry (Figure 1).[43] Therefore, dissociation of GTA is considered in the model for 85% RH. The OH oxidation rate constants for glutarate anions are based on the report by Wen et al.[44] In addition, because the hygroscopicity of inorganic salts is generally larger than that of organic materials,[48,49] the water uptake will also be enhanced in the presence of inorganic salts. The particle diameter (d_p) is a critical model input parameter, but the aqueous particle size was not directly monitored because aerosols were dried before the SEMS measurements. Thus, the aqueous particle sizes were calculated considering both the curvature effect and solution effect. For the solution effect, the equilibrium water activity of mixed organic-inorganic-water particles with varying mixing ratios was modeled using the AIOMFAC model;[50] for the curvature effect, the Kelvin equation is used:

$$e_{sc}(T) = e_s(T) \times \exp\left(\frac{4\sigma M_w}{RT\rho_w D}\right) \quad (3)$$

where $e_{sc}(T)$ and $e_s(T)$ are the equilibrium water vapor pressure over a curved and flat surface, M_w and ρ_w are the molecular weight and density of water, σ is the surface tension of the solution/air interface (σ = 0.072 J m^{-2}), R is the

https://doi.org/10.1021/acs.est.2c04670
Environ. Sci. Technol. 2022, 56, 15398−15407

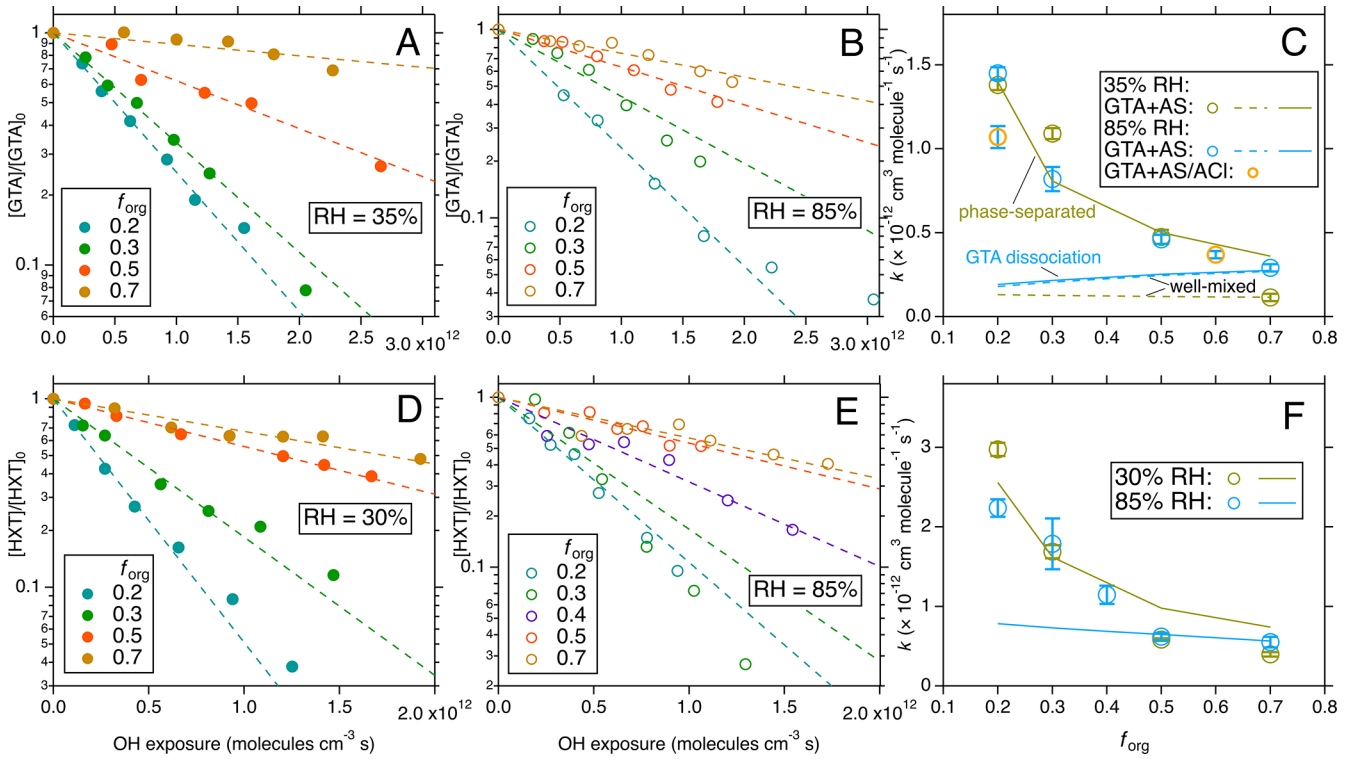

Figure 2. (A,B) Decay of GTA under 35 and 85% RH, respectively, with varied f_{org}. (C) Estimated oxidation rate constants as a function of f_{org} for GTA heterogeneous OH-oxidation. Curves represent model simulations under various assumptions. (D,E) Decay of HXT under 30 and 85% RH. (F) Estimated oxidation rate constants as a function of f_{org} for HXT heterogeneous OH-oxidation and corresponding model simulations. Dashed lines in A, B, D, and E are exponential fittings of the experimental data. In C and F, the error bars represent the standard deviation (1σ) of the fitted k; the curves are model simulations of the oxidation kinetics.

universal gas constant, T is the temperature, and D is the diameter of the droplet. Based on these two effects, given the RH and the amounts of organic and inorganic materials, the particle-phase water can be calculated. Thus, the particle's equilibrium wet size can be obtained. Figure S3 illustrates how the organic, inorganic, and water amounts vary with different f_{org} under 85% RH for GTA and HXT. As shown, the absorbed water dominates particle's volume under 85% RH especially for low f_{org}.

RESULTS AND DISCUSSION

OH-Initiated Heterogeneous Oxidation Kinetics of the Organic-Inorganic Mixed Aerosols. The (−)ESI-IMS-TOF measurements found no evidence for organosulfate formation in the oxidized aerosols for both GTA and HXT, suggesting that all the sulfate remains in its original inorganic form. Because sulfate can be derivatized and detected by GC-EI-MS and is not expected to react in the system, it is used as an "internal standard" to accurately quantify the degradation of GTA and HXT during the heterogeneous OH-oxidation. Additional tests verified that the GC-EI-MS peak intensity ratio of the organic material to sulfate is proportional to the mass ratio (Figure S4). The normalized intensities of GTA and HXT (after correction by the sulfate peak intensity) as a function of OH exposure are shown in Figure 2. The second-order rate constant (k) for the OH oxidation of GTA or HXT for each experimental condition is obtained by exponentially fitting the degradation data:

$$\frac{[\mathrm{Org}]}{[\mathrm{Org}]_0} = \exp(-k \times [\mathrm{OH}] \times t) \quad (4)$$

where $[\mathrm{Org}]_0$ and $[\mathrm{Org}]$ are the parent organic (GTA or HXT) peak intensity divided by the sulfate peak intensity in the GC-EI-MS measurements before and after oxidation, respectively; "$[\mathrm{OH}] \times t$" is the OH exposure. Interestingly, the decay rate constants for GTA (Figure 2A,B) and HXT (Figure 2D,E) are significantly larger when f_{org} are smaller under both low- and high-RH conditions. For GTA-AS particles, under 35% RH, the k for f_{org} = 0.2 (1.35×10^{-12} cm^3 molecule^{-1} s^{-1}) is ∼11 times larger than that for f_{org} = 0.7 (1.21×10^{-13} cm^3 molecule^{-1} s^{-1}); under 85% RH, the enhancement of k is not as much comparing f_{org} = 0.2 to 0.7, but still by a factor of ∼4 (Figure 2C). Similarly, for HXT-AS particles, the enhancement factor of k is ∼7 under low-RH conditions and ∼5 under high-RH conditions (Figure 2F). The causes for these largely different organic reactivities with varied f_{org} are examined in the discussion below.

Synergistic Role of RH, Inorganics, and Phase State on Organic Decay. Prior work suggested that GTA-AS mixed aerosols (1:1 molar ratio) have efflorescence RH (ERH) at 28−40% RH and HXT-AS mixed particles (1:1 molar ratio) have ERH at ∼ 47% RH.[51−54] Thus, we suggest that the organic-inorganic mixed aerosols in the FTR under 30−35% RH are likely efflorescent (or undergoing efflorescence). Previous studies provided comprehensive evidence that as the HXT-AS particles are dried to RH < 79.3%, they present clear phase separation with AS in the core and HXT in the outer shell.[54] In contrast, the phase state of mixed GTA-AS particles is less clear. It has been reported that mixed GTA-AS particles may not undergo a full phase separation; instead, they would lead to spatial separation with GTA predominantly found in the outer region of the particles (i.e., an organic-rich

https://doi.org/10.1021/acs.est.2c04670
Environ. Sci. Technol. 2022, 56, 15398−15407

phase) during crystallization.[19] Our single-particle levitation analysis suggests that as the GTA-AS mixed aerosol particles are dried from aqueous droplets to 35% RH (and lower), the particles experience efflorescence, consistent with prior research.[51−53] Also, based on the monotonic change in the calculated size and RI and the lack of any significant changes in the fitting error or spectral structure, there was no indication of phase separation at higher RH (Figure S5A). Instead, continuous changes in properties were found with decreasing RH. This result also agrees with prior work.[19] As the RH was increased from this dried state, the particles were observed to grow, as evidenced by the increase in the voltage required to balance the particles (Figure S5B). For crystalline particles, no measurable growth is typically observed until the deliquescence RH. In these mixed particles, growth indicates the presence of an amorphous phase (most likely rich in GTA), which allows for reversible uptake and loss of water. At the deliquescence RH, the crystalline regions of the particle (most likely rich in AS) dissolve and a significant increase in size is observed. Based on these observations, we suggest that for the AS + GTA system at low RH, the particles exist in a multiphase mixture of amorphous organic rich material and crystalline inorganic-rich material.

Although the phase states between the GTA-AS and HXT-AS systems are different under low-RH conditions (i.e., organic-rich amorphous phase vs. phase separation), the effect of f_{org} on heterogeneous OH-oxidation kinetics seems very similar (Figure 2C vs Figure 2F). To further investigate the aerosol phase state, we use the kinetic model to simulate the organic decay rate constants. In these simulations, the single tuning parameter α was adjusted to achieve the best fitted results for all the observed k values for each mixed aerosol system. For the low-RH conditions of the GTA-AS system, two model scenarios are probed. The first scenario assumes that the GTA-AS aerosols are well mixed under all the studied f_{org} conditions. Under this assumption, the bulk D_{org} for f_{org} = 0.2 is predicted to be ∼2 orders of magnitude larger than that for f_{org} = 0.7 (2.1×10^{-8} vs. 5.4×10^{-10} cm^2 s^{-1}). The faster diffusion in the particles leads to a small enhancement in the modeled k, given the same α and thus the same k_{ads} (Figure 2C). However, this enhancement is insufficient to explain the measurements. The second scenario assumes that the GTA-AS aerosols are fully phase-separated, thus exhibiting a core-shell structure with GTA coating on the AS core. Under this assumption, D_{org} in the GTA shell does not change with f_{org}, but the increased surface-to-volume ratio with decreased f_{org} could largely elevate the oxidation rate constant, consistent with the work by Lim et al.[21] In this scenario, the enhanced measurement of k with decreased f_{org} is better captured by the model, except for the f_{org} = 0.7 condition where the phase separation model greatly overpredicts the k (Figure 2C). Therefore, we suggest that when GTA dominates (e.g., f_{org} = 0.7), the GTA-AS particles' phase state is more likely well mixed, in which particle's diffusion may not be rapid enough to facilitate the material exchanges between particle surface and interior, causing the small k. When the inorganic fraction increases, the ERH of the mixed system will increase[17] and the particle phase state will shift toward efflorescence, which will favor a salt-out state and enhance the surface enrichment of organics. Thus, it is possible that the GTA-AS particles present an amorphous state between well-mixed and core-shell structures. This phase change is deepened by the decreased f_{org}, which largely enhances k. The amorphous phase state, unfortunately, cannot be applied in the model because the organic/inorganic mixing ratio gradients at different particle layers and with different f_{org} are unknown. However, it can be expected that with the phase state change, the simulated k could be more distinct between low- and high-f_{org} and the simulations could agree with the measurements better than the core-shell assumptions under all the f_{org} conditions. In the case of the HXT-AS mixed aerosols, the phase state model also better simulates the varied k under low-RH conditions (Figure 2F).

Under 85% RH, both the GTA-AS and HXT-AS systems are believed to exhibit a well-mixed aqueous state under all the f_{org} conditions,[17,55] in which the particle bulk diffusion is likely rapid enough (D_{org} on the order of 10^{-6} cm^2 s^{-1}) to free the surface renewal processes. With the model that treats the organic-inorganic aerosols as a well-mixed system, it predicts a fairly flat k as a function of f_{org} (Figure 2C,F). Since the anions of GTA (i.e., the glutarate monoanion and dianion) react faster with OH than GTA by a factor of two or so,[44] the kinetic model considers GTA dissociation (pKa1 = 4.35 and pKa2 = 5.42) in the aqueous aerosols and OH reactions with the anions. The pH of the aqueous GTA-AS aerosols under all the f_{org} conditions is estimated to be 2.9−3.4, suggesting that about 4−12% of GTA may dissociate into its monoanion, while further dissociation to the dianion is negligible. However, after implementing instantaneous GTA dissociation, the model only has a marginal change in the simulation results and still cannot explain the large gap in k (Figure 2C). For the HXT-AS system where acid dissociation is irrelevant, the k variation with f_{org} is clearly due to other reasons.

Hence, a few possible explanations are considered, including sulfate radical formation[56,57] and oxidation[58] as well as ionic strength accelerating the heterogenous OH oxidation.[59] To examine these possibilities, two additional 85%-RH experiments with GTA and mixed AS and ACl were performed, in which the f_{org} were controlled at 0.2 and 0.6, while the AS mass fraction was maintained constant at 0.2. As shown in Figure 2C, the two GTA + AS/ACl experiments exhibit similar GTA oxidation kinetics as the GTA + AS experiments, ruling out a unique role of sulfate promoting the heterogeneous oxidation kinetics. Moreover, the ionic strengths (I) of the two GTA + AS/ACl systems are similar (i.e., I = 4.2 M and 3.4 M for f_{org} = 0.2 and 0.6, respectively) and both lower than those in the GTA + AS experiments (4.1−8.5 M). This suggests that ionic strength is not the main reason for the distinct k with different f_{org}. Thus, a more plausible explanation comes from the surface propensity of organics, as evidenced by previous studies measuring the decreased surface tension of aqueous GTA aerosol particles.[60] At low f_{org} and high inorganic concentrations, which enhance the salting-out effect, more of the organic molecules will be present at the aqueous aerosol surface than a simple compositional mixing rule would indicate. This leads to a surface enrichment of organic molecules under all the experiment conditions explored in this study, even in the absence of a definitive liquid-liquid phase separation. With the high surface-to-volume ratios and rapid diffusion, this process allows for more efficient organic oxidation at the aerosol surface under lower f_{org}. The surface propensity of the organics also increases the likelihood of the adsorbed OH to collide and react with the interfacial organic molecules before desorption. In general, if a colliding OH molecule does not find an organic molecule to react at the particle surface, it is likely to desorb and evaporate, considering its very short lifetime on aqueous surfaces.[61] These results

https://doi.org/10.1021/acs.est.2c04670
Environ. Sci. Technol. 2022, 56, 15398−15407

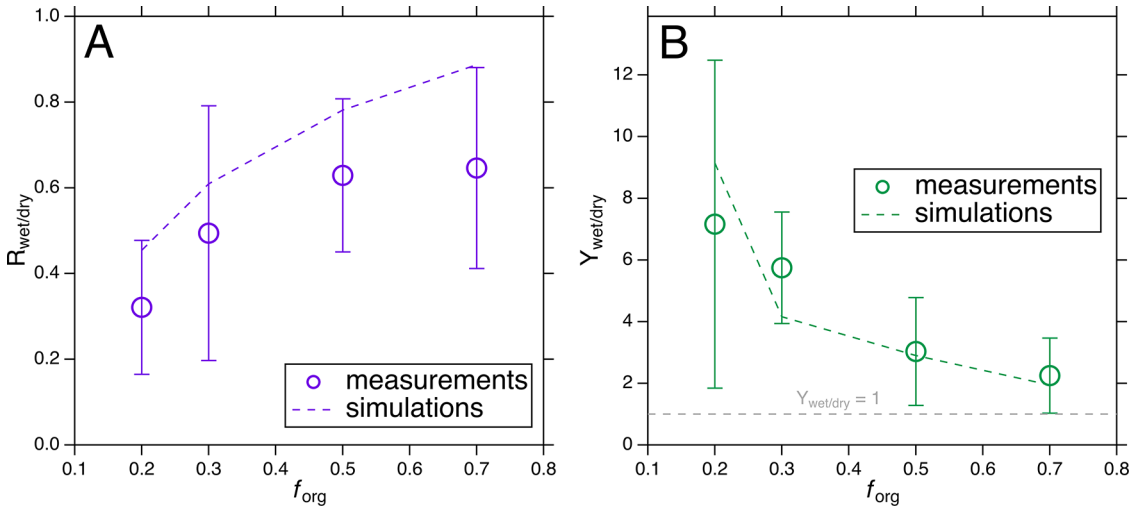

Figure 3. (A) Intensity ratios of the total hydroxyglutaric acids to total ketoglutaric acids compared between the high- and low-RH conditions ($R_{wet/dry}$) as a function of f_{org}. (B) Ratios of the total C_2-C_4 diacid yields between the high- and low-RH conditions ($Y_{wet/dry}$) as a function of f_{org}. Error bars represent the standard deviations of the measurements, and model simulations (colored dashed lines) are compared with the measurements.

underscore that for organic-inorganic mixed aerosols, the complex coupling of RH, phase state, and organic/inorganic fractions may largely impact the kinetics of heterogeneous oxidation under both low- and high-RH conditions. This also indicates that kinetic measurements from pure organic heterogeneous oxidation experiments may not be directly appliable to atmospheric aerosols, as they are often mixtures of organics and inorganics.

Reaction Pathways and Aerosol Composition Affected by RH and Phase State. As shown in Figure 1, the heterogeneous oxidation of organic particles by OH is initiated by abstraction of a hydrogen atom to produce an alkyl radical.[9,22] The alkyl radical then quickly reacts with oxygen to form RO_2. This hydrogen abstraction by OH can occur at different available C−H sites on the organic particles, which is evidenced by the isomers in the oxidation products. RO_2 can undergo self-reactions to form a ketone and an alcohol oxidation product via the Russell mechanism[62] and can also form RO. The RO may abstract a hydrogen atom from a neighboring organic molecule to form an alcohol, propagating free-radical cycling pathways. Alternatively, the RO may fragment by β-scission to form smaller products. Here, the oxidation of mixed GTA-AS particles is used as an example to demonstrate the dynamic RO pathways. As the GC-EI-MS chromatogram shown in Figure S6Aindicates, in addition to the two dominant peaks corresponding to sulfate (retention time, RT ∼ 11.5 min) and GTA (RT ∼ 19.1 min), many peaks are present as the oxidation products. The main functionalization products are the hydroxyglutaric acid isomers (RT = 23.9−24.1 min), the ketoglutaric acid isomers (RT = 24.7−25.1 min), and a few second-generation products (RT = 25.5−35 min). The main fragmentation products formed from RO cleavage detected by the GC-EI-MS are small diacids, including oxalic acid (RT ∼ 10.7 min), malonic acid (RT = 12.6 min), and succinic acid (RT = 16.0 min). Their detailed formation pathways can be found in Figure S7.

To gain further insights into the effects of the inorganic salts and RH on the reaction pathways, we explored the main functionalization products and fragmentation products under the studied RH and f_{org} conditions. In Figure 3A, the intensity ratios of the total hydroxyglutaric acids to total ketoglutaric acids (R) are compared between the high- and low-RH conditions under all the studied f_{org}, termed as $R_{wet/dry}$. Under each RH-f_{org} experiment, the variation of R is relatively small compared to that between different experiments. From Figure 3A, the $R_{wet/dry}$ appears to increase with f_{org} but is always smaller than 1 under the studied conditions, suggesting that the high-RH conditions lead to lower R than the low-RH conditions overall. As shown in Figure 1, both hydroxyglutaric acids and ketoglutaric acids can be formed from the Russell mechanism at a 1:1 ratio, while hydroxyglutaric acids may also be formed from the reactions of GTA-derived RO with another organic molecule (i.e., the chain propagation chemistry). Hence, the decreasing $R_{wet/dry}$ under lower f_{org} suggests that the RO-mediated chain propagation chemistry is inhibited due to the dilution of organics by both particle water and inorganic salts in the mixed aerosols (see Figure S3).

In comparison to the results for the functionalization products, the fragmentation products measured by the GC-EI-MS (i.e., the C_2-C_4 diacids) exhibit the opposite trend with enhanced formation under high-RH conditions. Figure 3B presents the ratios of the total C_2-C_4 diacid yields between the high- and low-RH conditions under all the studied f_{org}, termed as $Y_{wet/dry}$. Here, the total C_2-C_4 diacid yields are estimated by the total mass of C_2-C_4 diacids over reacted GTA mass, all quantified with authentic standards. As shown in Figure 3B, $Y_{wet/dry}$ under all the studied f_{org} conditions is higher than 1, suggesting that RO fragmentation is enhanced under high-RH conditions overall. Further, $Y_{wet/dry}$ exhibits a decreasing trend with increased f_{org} (in opposition to $R_{wet/dry}$ in Figure 3A), suggesting that the dilution of organics by particle water and inorganic salts in the mixed aerosols favors RO decomposition by a factor of 3 to 4. In addition, the auxiliary IMS-TOF measurements also show that the relative intensities of major fragmentation products do not vary significantly between different RH and f_{org} conditions (Figure S8), indicating that the differences shown in Figure 3B are representative of all the fragmentation products. Therefore, the findings presented in Figure 3 suggest that the competing pathways of RO undergoing the secondary chain chemistry versus fragmenta-

https://doi.org/10.1021/acs.est.2c04670
Environ. Sci. Technol. 2022, 56, 15398−15407

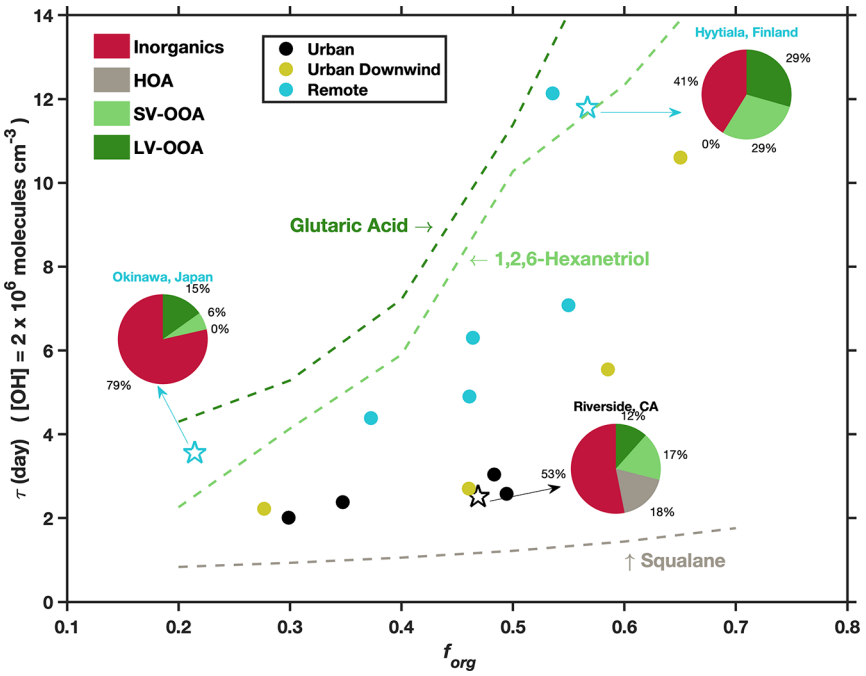

Figure 4. Estimated organic aerosol oxidation lifetime versus f_{org} at different locations. The compositional data are from the aerosol mass spectrometer measurements from the work by Jimenez et al.[1] for nonrefractive submicron particles. Each dot or pentagram represents a location, and the color indicates the type of sampling location: urban areas (black), <100 miles downwind of major cities (yellow-green), and rural/remote areas >100 miles downwind (cyan). The pie charts show the compositional contributions to total aerosols for three representative locations. The dashed lines trace the experimental results in this work.

tion are greatly impacted by the presence of inorganic material and particle water. Under high-RH conditions, inorganic materials more prominently absorb water, which largely reduces organic concentrations in the particles and increases organic distance in the nanoscale. For instance, with RH = 85% and f_{org} = 0.2, GTA only makes ~6.6% (volume fraction) in the particles and the rest are AS and water (Figure S3). The addition of water further separates the neighboring organic molecules and inhibits the secondary chemistry (bimolecular reactions), while the RO unimolecular decomposition is unaffected and thus favored under these conditions. This transition in reaction pathways is deepened by decreased f_{org}, which leads to more water absorption and greater dilution of organics in the particle phase.

The model simulations exhibit consistent trends with the measurements shown in Figure 3. Here, the low-RH condition model assumes phase separation of GTA-AS aerosols with the same model setup, as shown in Figure 2C, whereas the high-RH condition model uses varied α values at different f_{org} to match GTA oxidation kinetics. The resultant simulated $R_{wet/dry}$ and $Y_{wet/dry}$ reasonably agree with the measurements within uncertainty, suggesting that the proposed explanation of the reduced formation of hydroxyglutaric acids and enhanced RO fragmentation products under high RH and low f_{org} is plausible. The products from HXT oxidation are not as comprehensively characterized as for GTA due to the multiple −OH groups complicating the EI mass spectral interpretation. Nevertheless, a product that is clearly identified from HXT oxidation under f_{org} = 0.5 and 0.7 is 5-hydroxypentanoic acid (see Figure S6B for the representative GC-EI-MS chromatogram), which is expected to form from hydrogen abstraction on the tertiary carbon of HXT followed by the tertiary RO decomposition (see the mechanism in Figure S9). The formation yields of this major fragmentation product show very similar behavior to those for the GTA fragmentation products (Figure S9), suggesting that the impact of inorganic salts and the associated particle water on RO pathways is a common effect, rather than only for GTA.

■ ATMOSPHERIC IMPLICATIONS

To further examine the impacts of the presence of inorganic salts on the organic aerosol decay against heterogeneous OH oxidation for atmospheric particles, we applied our experimental kinetic results to the aerosol bulk compositional datasets collected at different locations around the world in the past decades by aerosol mass spectrometers.[1,16] For each location, the compositions are categorized into inorganics and organics. The organics can be further divided into hydrocarbon-like organic aerosol (HOA), semivolatile oxygenated organic aerosol (SV-OOA), and low-volatile oxygenated organic aerosol (LV-OOA). f_{org} at these locations varied from 0.2 to 0.7, which are within our experimental conditions. Based on the O/C ratios, we use GTA as a surrogate for the LV-OOA and HXT for the SV-OOA. For the HOA, we adopt the squalane kinetic data from previous research.[21] The corresponding f_{org}-dependent second-order rate constants k were also applied to approximate oxidation kinetics of HOA, SV-OOA, and LV-OOA. It is well understood that this is a highly simplified approach and atmospheric organic aerosols are much more complex with possibly a wide range of oxidation kinetics for each of these categories. However, we expect that the phase state behavior of species under HOA, SV-OOA, and LV-OOA is likely similar to that of squalane, HXT, and GTA. Thus, we suggest that the relative variations of their oxidation kinetics with f_{org} and RH can be compared. For SV-OOA and LV-OOA, we also use the RH-dependent kinetic results from this work; for HOA, we expect that RH plays a small role in their oxidation kinetics. Thus, the overall

https://doi.org/10.1021/acs.est.2c04670
Environ. Sci. Technol. 2022, 56, 15398−15407

oxidation rate constant k for the bulk organics can then be calculated from the mass-weighted mean of all these components. From the calculated k, the organic lifetime τ ($1/k$[OH]) can also be obtained assuming an average [OH] concentration of 2×10^6 molecules cm^{-3}.[63] The results of the organic lifetime for different compositions under low-RH conditions are shown in Figure 4 and under high-RH conditions in Figure S10. It should be noted that in this simplified approximation, internal mixing among HOA, SV-OOA, and LV-OOA is assumed, while some laboratory and field studies have shown that HOA do not always mix with OOA.[64,65] Nevertheless, combining the results from this work and that of Lim et al.,[21] it appears that higher inorganic fractions accelerate organic aerosol oxidation to similar extents regardless of whether they are mixed or not. However, future studies are warranted to examine ternary systems (i.e., HOA-OOA-inorganics).

As presented in Figure 4, the lifetime of organics could be shortened dramatically when mixed with higher fractions of inorganic salts. For example, at Okinawa, Japan, organics account for about only 21% of the total fine aerosol mass and the organic lifetime is ~3 days. On the contrary, at the location of Hyytiala, Finland, the organic mass accounts for about 58% and the organic lifetime is ~12 days. The organic lifetime in organic-rich areas can be four times longer than that in inorganic-rich areas. This f_{org}-dependent trend is consistent for similar locations (i.e., urban, urban downwind, or remote). A similar enhanced organic decay caused by inorganic salts is present under both low-RH (Figure 4) and high-RH conditions (Figure S10). This comparison underscores the importance of inorganic salts on the estimation of the atmospheric organic lifetime against heterogeneous OH oxidation, and the kinetic studies using pure organic materials will lead to longer lifetimes of organic aerosol in the atmosphere. Based on the results of this work, we also expect similar effects on organic aerosol oxidation timescale under RH in the studied range (i.e., 30−80%) and in the presence of other inorganic salts (e.g., nitrate). Nevertheless, future studies are needed to prove this hypothesis.

In addition to the organic oxidation kinetics, analysis of the experimental oxidation products also reveals that the dilution effect caused by the increased inorganic fraction and corresponding enhanced water uptake under high-RH conditions will inhibit secondary chemistry driven by RO and promote the RO decomposition pathway to form more volatile fragmentation products, which will result in a larger degree of evaporation.[66] Thus, the gas-particle distribution of organics will also be largely impacted.

■ ASSOCIATED CONTENT

Supporting Information

The Supporting Information is available free of charge at https://pubs.acs.org/doi/10.1021/acs.est.2c04670.

Additional experimental setup and model details (PDF)

■ AUTHOR INFORMATION

Corresponding Author

Haofei Zhang − *Department of Chemistry, University of California, Riverside, California 92507, United States;* orcid.org/0000-0002-7936-4493; Email: haofei.zhang@ucr.edu

Authors

Chuanyang Shen − *Department of Chemistry, University of California, Riverside, California 92507, United States*

Wen Zhang − *Department of Chemistry, University of California, Riverside, California 92507, United States*

Jack Choczynski − *Department of Chemistry, University of California, Riverside, California 92507, United States*

James F. Davies − *Department of Chemistry, University of California, Riverside, California 92507, United States;* orcid.org/0000-0002-7415-3638

Complete contact information is available at: https://pubs.acs.org/10.1021/acs.est.2c04670

Notes

The authors declare no competing financial interest.

■ ACKNOWLEDGMENTS

This work was supported by National Science Foundation (CHE-2002413). J.F.D. and J.C. acknowledge the support of the National Science Foundation (CHE- 2108004).

■ REFERENCES

(1) Jimenez, J. L.; Canagaratna, M.; Donahue, N.; Prevot, A.; Zhang, Q.; Kroll, J. H.; DeCarlo, P. F.; Allan, J. D.; Coe, H.; Ng, N.; Aiken, A. C.; Docherty, K. S.; Ulbrich, I. M.; Grieshop, A. P.; Robinson, A. L.; Duplissy, J.; Smith, J. D.; Wilson, K. R.; Lanz, V. A.; Hueglin, C.; Sun, Y. L.; Tian, J.; Laaksonen, A.; Raatikainen, T.; Rautiainen, J.; Vaattovaara, P.; Ehn, M.; Kulmala, M.; Tomlinson, J. M.; Collins, D. R.; Cubison, M. J.; Dunlea, J.; Huffman, J. A.; Onasch, T. B.; Alfarra, M. R.; Williams, P. I.; Bower, K.; Kondo, Y.; Schneider, J.; Drewnick, F.; Borrmann, S.; Weimer, S.; Demerjian, K.; Salcedo, D.; Cottrell, L.; Griffin, R.; Takami, A.; Miyoshi, T.; Hatakeyama, S.; Shimono, A.; Sun, J. Y.; Zhang, Y. M.; Dzepina, K.; Kimmel, J. R.; Sueper, D.; Jayne, J. T.; Herndon, S. C.; Trimborn, A. M.; Williams, L. R.; Wood, E. C.; Middlebrook, A. M.; Kolb, C. E.; Baltensperger, U.; Worsnop, D. R. Evolution of organic aerosols in the atmosphere. *science* **2009**, *326*, 1525−1529.

(2) George, I.; Abbatt, J. Heterogeneous oxidation of atmospheric aerosol particles by gas-phase radicals. *Nat. Chem.* **2010**, *2*, 713−722.

(3) Smith, J. D.; Kroll, J. H.; Cappa, C. D.; Che, D. L.; Liu, C. L.; Ahmed, M.; Leone, S. R.; Worsnop, D. R.; Wilson, K. R. The heterogeneous reaction of hydroxyl radicals with sub-micron squalane particles: a model system for understanding the oxidative aging of ambient aerosols. *Atmos. Chem. Phys.* **2009**, *9*, 3209−3222.

(4) He, Q.; Tomaz, S.; Li, C.; Zhu, M.; Meidan, D.; Riva, M.; Laskin, A.; Brown, S. S.; George, C.; Wang, X.; Rudich, Y. Optical Properties of Secondary Organic Aerosol Produced by Nitrate Radical Oxidation of Biogenic Volatile Organic Compounds. *Environmental Science & Technology* **2021**, *55*, 2878−2889.

(5) George, I. J.; Chang, R. Y. W.; Danov, V.; Vlasenko, A.; Abbatt, J. P. D. Modification of cloud condensation nucleus activity of organic aerosols by hydroxyl radical heterogeneous oxidation. *Atmos. Environ.* **2009**, *43*, 5038−5045.

(6) Cappa, C. D.; Che, D. L.; Kessler, S. H.; Kroll, J. H.; Wilson, K. R.Variations in organic aerosol optical and hygroscopic properties upon heterogeneous OH oxidation. *Journal of Geophysical Research: Atmospheres***2011**, *116*(). DOI: 10.1029/2011jd015918

(7) Petters, M. D.; Prenni, A. J.; Kreidenweis, S. M.; DeMott, P. J.; Matsunaga, A.; Lim, Y. B.; Ziemann, P. J.Chemical aging and the hydrophobic-to-hydrophilic conversion of carbonaceous aerosol. *Geophys. Res. Lett.***2006**, *33*(). DOI: 10.1029/2006gl027249

(8) Kroll, J. H.; Smith, J. D.; Che, D. L.; Kessler, S. H.; Worsnop, D. R.; Wilson, K. R. Measurement of fragmentation and functionalization pathways in the heterogeneous oxidation of oxidized organic aerosol. *Physical chemistry chemical physics : PCCP* **2009**, *11*, 8005−8014.

(9) Chan, M. N.; Zhang, H.; Goldstein, A. H.; Wilson, K. R. Role of Water and Phase in the Heterogeneous Oxidation of Solid and Aqueous Succinic Acid Aerosol by Hydroxyl Radicals. *J. Phys. Chem. C* **2014**, *118*, 28978−28992.
(10) Kessler, S. H.; Nah, T.; Daumit, K. E.; Smith, J. D.; Leone, S. R.; Kolb, C. E.; Worsnop, D. R.; Wilson, K. R.; Kroll, J. H. OH-initiated heterogeneous aging of highly oxidized organic aerosol. *J. Phys. Chem. A* **2012**, *116*, 6358−6365.
(11) Kessler, S. H.; Smith, J. D.; Che, D. L.; Worsnop, D. R.; Wilson, K. R.; Kroll, J. H. Chemical sinks of organic aerosol: kinetics and products of the heterogeneous oxidation of erythritol and levoglucosan. *Environ. Sci. Technol.* **2010**, *44*, 7005−7010.
(12) Slade, J. H.; Knopf, D. A. Multiphase OH oxidation kinetics of organic aerosol: The role of particle phase state and relative humidity. *Geophys. Res. Lett.* **2014**, *41*, 5297−5306.
(13) Chapleski, R. C.; Zhang, Y.; Troya, D.; Morris, J. R. Heterogeneous chemistry and reaction dynamics of the atmospheric oxidants, O3, NO3, and OH, on organic surfaces. *Chem. Soc. Rev.* **2016**, *45*, 3731−3746.
(14) Zhao, Z.; Mayorga, R.; Lee, J.; Yang, X.; Tolentino, R.; Zhang, W.; Vuong, A.; Zhang, H. Site-Specific Mechanisms in OH-Initiated Organic Aerosol Heterogeneous Oxidation Revealed by Isomer-Resolved Molecular Characterization. *ACS Earth Space Chem* **2020**, *4*, 783−794.
(15) Zhao, Z.; Tolentino, R.; Lee, J.; Vuong, A.; Yang, X.; Zhang, H. Interfacial Dimerization by Organic Radical Reactions during Heterogeneous Oxidative Aging of Oxygenated Organic Aerosols. *J. Phys. Chem. A* **2019**, *123*, 10782−10792.
(16) Zhang, Q.; Jimenez, J. L.; Canagaratna, M.; Allan, J. D.; Coe, H.; Ulbrich, I.; Alfarra, M.; Takami, A.; Middlebrook, A.; Sun, Y.Ubiquity and dominance of oxygenated species in organic aerosols in anthropogenically-influenced Northern Hemisphere midlatitudes. *Geophys. Res. Lett.***2007**, *34*(). DOI: 10.1029/2007gl029979
(17) Bertram, A. K.; Martin, S. T.; Hanna, S. J.; Smith, M. L.; Bodsworth, A.; Chen, Q.; Kuwata, M.; Liu, A.; You, Y.; Zorn, S. R. Predicting the relative humidities of liquid-liquid phase separation, efflorescence, and deliquescence of mixed particles of ammonium sulfate, organic material, and water using the organic-to-sulfate mass ratio of the particle and the oxygen-to-carbon elemental ratio of the organic component. *Atmos. Chem. Phys.* **2011**, *11*, 10995−11006.
(18) Svenningsson, B.; Rissler, J.; Swietlicki, E.; Mircea, M.; Bilde, M.; Facchini, M. C.; Decesari, S.; Fuzzi, S.; Zhou, J.; Mønster, J.; Rosenørn, T. Hygroscopic growth and critical supersaturations for mixed aerosol particles of inorganic and organic compounds of atmospheric relevance. *Atmos. Chem. Phys.* **2006**, *6*, 1937−1952.
(19) Peckhaus, A.; Grass, S.; Treuel, L.; Zellner, R. Deliquescence and Efflorescence Behavior of Ternary Inorganic/Organic/Water Aerosol Particles. *J. Phys. Chem. A* **2012**, *116*, 6199−6210.
(20) Veghte, D. P.; Altaf, M. B.; Freedman, M. A. Size dependence of the structure of organic aerosol. *J. Am. Chem. Soc.* **2013**, *135*, 16046−16049.
(21) Lim, C. Y.; Browne, E. C.; Sugrue, R. A.; Kroll, J. H. Rapid heterogeneous oxidation of organic coatings on submicron aerosols. *Geophys. Res. Lett.* **2017**, *44*, 2949−2957.
(22) Lam, H. K.; Shum, S. M.; Davies, J. F.; Song, M.; Zuend, A.; Chan, M. N. Effects of inorganic salts on the heterogeneous OH oxidation of organic compounds: insights from methylglutaric acid−ammonium sulfate. *Atmos. Chem. Phys.* **2019**, *19*, 9581−9593.
(23) Chen, Y.; Zhang, Y.; Lambe, A. T.; Xu, R.; Lei, Z.; Olson, N. E.; Zhang, Z.; Szalkowski, T.; Cui, T.; Vizuete, W.; Gold, A.; Turpin, B. J.; Ault, A. P.; Chan, M. N.; Surratt, J. D. Heterogeneous Hydroxyl Radical Oxidation of Isoprene-Epoxydiol-Derived Methyltetrol Sulfates: Plausible Formation Mechanisms of Previously Unexplained Organosulfates in Ambient Fine Aerosols. *Environ. Sci. Technol. Lett.* **2020**, *7*, 460−468.
(24) McNeill, V. F.; Yatavelli, R. L. N.; Thornton, J. A.; Stipe, C. B.; Landgrebe, O. Heterogeneous OH oxidation of palmitic acid in single component and internally mixed aerosol particles: vaporization and the role of particle phase. *Atmos. Chem. Phys.* **2008**, *8*, 5465−5476.
(25) Dennis-Smither, B. J.; Miles, R. E. H.; Reid, J. P.Oxidative aging of mixed oleic acid/sodium chloride aerosol particles. *J. Geophys. Res.: Atmos.***2012**, *117*(). DOI: 10.1029/2012jd018163
(26) Song, M.; Marcolli, C.; Krieger, U. K.; Lienhard, D. M.; Peter, T. Morphologies of mixed organic/inorganic/aqueous aerosol droplets. *Faraday Discuss.* **2013**, *165*, 289−316.
(27) Ye, Q.; Gu, P.; Li, H. Z.; Robinson, E. S.; Lipsky, E.; Kaltsonoudis, C.; Lee, A. K. Y.; Apte, J. S.; Robinson, A. L.; Sullivan, R. C.; Presto, A. A.; Donahue, N. M. Spatial Variability of Sources and Mixing State of Atmospheric Particles in a Metropolitan Area. *Environmental Science & Technology* **2018**, *52*, 6807−6815.
(28) McNeill, V. F.; Wolfe, G. M.; Thornton, J. A. The Oxidation of Oleate in Submicron Aqueous Salt Aerosols: Evidence of a Surface Process. *J. Phys. Chem. A* **2007**, *111*, 1073−1083.
(29) Russell, L. M.; Bahadur, R.; Ziemann, P. J. Identifying organic aerosol sources by comparing functional group composition in chamber and atmospheric particles. *Proc. Natl. Acad. Sci. U.S.A.* **2011**, *108*, 3516−3521.
(30) Faust, J. A.; Abbatt, J. P. Organic surfactants protect dissolved aerosol components against heterogeneous oxidation. *J. Phys. Chem. A* **2019**, *123*, 2114−2124.
(31) Krechmer, J. E.; Groessl, M.; Zhang, X.; Junninen, H.; Massoli, P.; Lambe, A. T.; Kimmel, J. R.; Cubison, M. J.; Graf, S.; Lin, Y. H.; Budisulistiorini, S. H.; Zhang, H.; Surratt, J. D.; Knochenmuss, R.; Jayne, J. T.; Worsnop, D. R.; Jimenez, J. L.; Canagaratna, M. R. Ion mobility spectrometry−mass spectrometry (IMS−MS) for on- and offline analysis of atmospheric gas and aerosol species. *Atmos. Meas. Tech.* **2016**, *9*, 3245−3262.
(32) Santos, F. J.; Galceran, M. T. Modern developments in gas chromatography−mass spectrometry-based environmental analysis. *J. Chromatogr. A* **2003**, *1000*, 125−51.
(33) Mayorga, R. J.; Zhao, Z.; Zhang, H. Formation of secondary organic aerosol from nitrate radical oxidation of phenolic VOCs: Implications for nitration mechanisms and brown carbon formation. *Atmos. Environ.* **2021**, *244*, 117910.
(34) Zhao, Z.; Le, C.; Xu, Q.; Peng, W.; Jiang, H.; Lin, Y.-H.; Cocker, D. R.; Zhang, H. Compositional Evolution of Secondary Organic Aerosol as Temperature and Relative Humidity Cycle in Atmospherically Relevant Ranges. *ACS Earth Space Chem* **2019**, *3*, 2549−2558.
(35) Zhao, Z.; Yang, X.; Lee, J.; Tolentino, R.; Mayorga, R.; Zhang, W.; Zhang, H. Diverse reactions in highly functionalized organic aerosols during thermal desorption. *ACS Earth Space Chem.* **2019**, *4*, 283−296.
(36) Price, C. L.; Bain, A.; Wallace, B. J.; Preston, T. C.; Davies, J. F. Simultaneous Retrieval of the Size and Refractive Index of Suspended Droplets in a Linear Quadrupole Electrodynamic Balance. *J. Phys. Chem. A* **2020**, *124*, 1811−1820.
(37) Davies, J. F. Mass, charge, and radius of droplets in a linear quadrupole electrodynamic balance. *Aerosol Sci. Technol.* **2019**, *53*, 309−320.
(38) Shiraiwa, M.; Pfrang, C.; Koop, T.; Pöschl, U. Kinetic multi-layer model of gas-particle interactions in aerosols and clouds (KM-GAP): linking condensation, evaporation and chemical reactions of organics, oxidants and water. *Atmos. Chem. Phys.* **2012**, *12*, 2777−2794.
(39) Houle, F. A.; Hinsberg, W. D.; Wilson, K. R. Oxidation of a model alkane aerosol by OH radical: the emergent nature of reactive uptake. *Phys. Chem. Chem. Phys.* **2015**, *17*, 4412−4423.
(40) Wiegel, A. A.; Liu, M. J.; Hinsberg, W. D.; Wilson, K. R.; Houle, F. A. Diffusive confinement of free radical intermediates in the OH radical oxidation of semisolid aerosols. *Physical chemistry chemical physics : PCCP* **2017**, *19*, 6814−6830.
(41) Zuend, A.; Marcolli, C.; Luo, B. P.; Peter, T. A thermodynamic model of mixed organic-inorganic aerosols to predict activity coefficients. *Atmos. Chem. Phys.* **2008**, *8*, 4559−4593.
(42) Gervasi, N. R.; Topping, D. O.; Zuend, A. A predictive group-contribution model for the viscosity of aqueous organic aerosol. *Atmos. Chem. Phys.* **2020**, *20*, 2987−3008.

(43) Liu, M. J.; Wiegel, A. A.; Wilson, K. R.; Houle, F. A. Aerosol Fragmentation Driven by Coupling of Acid−Base and Free-Radical Chemistry in the Heterogeneous Oxidation of Aqueous Citric Acid by OH Radicals. *J. Phys. Chem. A* **2017**, *121*, 5856−5870.
(44) Wen, L.; Schaefer, T.; He, L.; Zhang, Y.; Sun, X.; Ventura, O. N.; Herrmann, H. T- and pH-Dependent Kinetics of the Reactions of ·OH(aq) with Glutaric and Adipic Acid for Atmospheric Aqueous-Phase Chemistry. *ACS Earth Space Chem* **2021**, *5*, 1854−1864.
(45) Doussin, J. F.; Monod, A. Structure−activity relationship for the estimation of OH-oxidation rate constants of carbonyl compounds in the aqueous phase. *Atmos. Chem. Phys.* **2013**, *13*, 11625−11641.
(46) Monod, A.; Doussin, J. F. Structure-activity relationship for the estimation of OH-oxidation rate constants of aliphatic organic compounds in the aqueous phase: alkanes, alcohols, organic acids and bases. *Atmos. Environ.* **2008**, *42*, 7611−7622.
(47) Richards-Henderson, N. K.; Goldstein, A. H.; Wilson, K. R. Large Enhancement in the Heterogeneous Oxidation Rate of Organic Aerosols by Hydroxyl Radicals in the Presence of Nitric Oxide. *J. Phys. Chem. Lett.* **2015**, *6*, 4451−4455.
(48) Kuang, Y.; Xu, W.; Tao, J.; Ma, N.; Zhao, C.; Shao, M. A Review on Laboratory Studies and Field Measurements of Atmospheric Organic Aerosol Hygroscopicity and Its Parameterization Based on Oxidation Levels. *Current Pollution Reports* **2020**, *6*, 410−424.
(49) Petters, M. D.; Kreidenweis, S. M. A single parameter representation of hygroscopic growth and cloud condensation nucleus activity − Part 2: Including solubility. *Atmos. Chem. Phys.* **2008**, *8*, 6273−6279.
(50) Zuend, A.; Marcolli, C.; Booth, A. M.; Lienhard, D. M.; Soonsin, V.; Krieger, U. K.; Topping, D. O.; McFiggans, G.; Peter, T.; Seinfeld, J. H. New and extended parameterization of the thermodynamic model AIOMFAC: calculation of activity coefficients for organic-inorganic mixtures containing carboxyl, hydroxyl, carbonyl, ether, ester, alkenyl, alkyl, and aromatic functional groups. *Atmos. Chem. Phys.* **2011**, *11*, 9155−9206.
(51) Lee, A. K. Y.; Ling, T. Y.; Chan, C. K. Understanding hygroscopic growth and phase transformation of aerosols using single particle Raman spectroscopy in an electrodynamic balance. *Faraday Discuss.* **2008**, *137*, 245−263.
(52) Ling, T. Y.; Chan, C. K.Partial crystallization and deliquescence of particles containing ammonium sulfate and dicarboxylic acids. *J. Geophys. Res. Atmos.***2008**, *113*(). DOI: 10.1029/2008jd009779
(53) Zardini, A. A.; Sjogren, S.; Marcolli, C.; Krieger, U. K.; Gysel, M.; Weingartner, E.; Baltensperger, U.; Peter, T. A combined particle trap/HTDMA hygroscopicity study of mixed inorganic/organic aerosol particles. *Atmos. Chem. Phys.* **2008**, *8*, 5589−5601.
(54) Ma, S.; Chen, Z.; Pang, S.; Zhang, Y. Observations on hygroscopic growth and phase transitions of mixed 1, 2, 6-hexanetriol / (NH4)2SO4 particles: investigation of the liquid−liquid phase separation (LLPS) dynamic process and mechanism and secondary LLPS during the dehumidification. *Atmos. Chem. Phys.* **2021**, *21*, 9705−9717.
(55) Cruz, C. N.; Pandis, S. N. Deliquescence and hygroscopic growth of mixed inorganic− organic atmospheric aerosol. *Environmental Science & Technology* **2000**, *34*, 4313−4319.
(56) Tang, Y.; Thorn, R. P.; Mauldin, R. L.; Wine, P. H. Kinetics and spectroscopy of the SO4− radical in aqueous solution. *J. Photochem. Photobiol., A* **1988**, *44*, 243−258.
(57) Hayon, E.; McGarvey, J. J. Flash photolysis in the vacuum ultraviolet region of sulfate, carbonate, and hydroxyl ions in aqueous solutions. *J. Phys. Chem.* **1967**, *71*, 1472−1477.
(58) Kwong, K. C.; Chim, M. M.; Davies, J. F.; Wilson, K. R.; Chan, M. N. Importance of sulfate radical anion formation and chemistry in heterogeneous OH oxidation of sodium methyl sulfate, the smallest organosulfate. *Atmos. Chem. Phys.* **2018**, *18*, 2809−2820.
(59) Mekic, M.; Wang, Y.; Loisel, G.; Vione, D.; Gligorovski, S. Ionic Strength Effect Alters the Heterogeneous Ozone Oxidation of Methoxyphenols in Going from Cloud Droplets to Aerosol Deliquescent Particles. *Environ. Sci. Technol.* **2020**, *54*, 12898−12907.
(60) Bzdek, B. R.; Power, R. M.; Simpson, S. H.; Reid, J. P.; Royall, C. P. Precise, contactless measurements of the surface tension of picolitre aerosol droplets. *Chem. Sci.* **2016**, *7*, 274−285.
(61) Vieceli, J.; Roeselová, M.; Potter, N.; Dang, L. X.; Garrett, B. C.; Tobias, D. J. Molecular Dynamics Simulations of Atmospheric Oxidants at the Air−Water Interface: Solvation and Accommodation of OH and O3. *J. Phys. Chem. B* **2005**, *109*, 15876−15892.
(62) Russell, G. A. Deuterium-isotope Effects in the Autoxidation of Aralkyl Hydrocarbons. Mechanism of the Interaction of PEroxy Radicals1. *J. Am. Chem. Soc.* **1957**, *79*, 3871−3877.
(63) Li, M.; Karu, E.; Brenninkmeijer, C.; Fischer, H.; Lelieveld, J.; Williams, J. Tropospheric OH and stratospheric OH and Cl concentrations determined from CH4, CH3Cl, and SF6 measurements. *npj Clim. Atmos. Sci.* **2018**, *1*, 29.
(64) Mahrt, F.; Huang, Y.; Zaks, J.; Devi, A.; Peng, L.; Ohno, P. E.; Qin, Y. M.; Martin, S. T.; Ammann, M.; Bertram, A. K. Phase Behavior of Internal Mixtures of Hydrocarbon-like Primary Organic Aerosol and Secondary Aerosol Based on Their Differences in Oxygen-to-Carbon Ratios. *Environ. Sci. Technol.* **2022**, *56*, 3960−3973.
(65) Huang, Y.; Mahrt, F.; Xu, S.; Shiraiwa, M.; Zuend, A.; Bertram, A. K. Coexistence of three liquid phases in individual atmospheric aerosol particles. *Proc. Natl. Acad. Sci., India, Sect. A* **2021**, *118*, No. e2102512118.
(66) Molina, M. J.; Ivanov, A. V.; Trakhtenberg, S.; Molina, L. T. Atmospheric evolution of organic aerosol. *Geophys. Res. Lett.* **2004**, *31*, n/a.

Recommended by ACS

Ionic Strength Enhances the Multiphase Oxidation Rate of Sulfur Dioxide by Ozone in Aqueous Aerosols: Implications for Sulfate Production in the Marine Atmosphere
Chen Yu, Aijun Ding, *et al.*
APRIL 11, 2023
ENVIRONMENTAL SCIENCE & TECHNOLOGY
READ

NH_3 Weakens the Enhancing Effect of SO_2 on Biogenic Secondary Organic Aerosol Formation
Lin Du, Maofa Ge, *et al.*
FEBRUARY 01, 2023
ENVIRONMENTAL SCIENCE & TECHNOLOGY LETTERS
READ

Synergistic Effects of SO_2 and NH_3 Coexistence on SOA Formation from Gasoline Evaporative Emissions
Tianzeng Chen, Hong He, *et al.*
APRIL 13, 2023
ENVIRONMENTAL SCIENCE & TECHNOLOGY
READ

Singlet Oxygen Seasonality in Aqueous PM_{10} is Driven by Biomass Burning and Anthropogenic Secondary Organic Aerosol
Sophie Bogler, Nadine Borduas-Dedekind, *et al.*
OCTOBER 28, 2022
ENVIRONMENTAL SCIENCE & TECHNOLOGY
READ

Get More Suggestions >